Research Article GU J Sci 38(1): x-x (2025) DOI: 10.35378/gujs.1479385

Gazi University

Journal of Science

http://dergipark.gov.tr/gujs

An Investigation of Structural, Optical and Pyroelectrical Properties of $LiTaO_3$

Mustafa BUYUKHARMAN[1,2*], Ahmet UNVERDI[1,2], Fahrettin SARCAN[1], Sule OZDILEK[2,3], Alican OKCUN[2], Ayse EROL[1]

[1] *Department of Physics, Faculty of Science, Istanbul University, TR-34134 Istanbul, Türkiye*
[2] *Department of Advanced R&D, Nero Industries, TR-06909 Ankara, Türkiye*
[3] *Department of Physics, Gebze Technical University, TR-41400 Kocaeli, Türkiye*

Highlights

- Structural, optical, and pyroelectric properties of bulk $LiTaO_3$ crystals is investigated
- The effect of sample size and thickness on pyroelectrical properties of $LiTaO_3$ is reported.
- The thinner $LiTaO_3$ generated larger pyroelectric current density.
- The bandgap of $LiTaO_3$ is determined as being direct and falls into deep UV region.

Article Info

Received: 02 Sep 2024
Accepted: 15 Oct 2024

Keywords

$LiTaO_3$,
Pyroelectricity
Pyroelectric current
IR detector
Pyroelectric material

Abstract

In this study, structural, optical, and pyroelectric properties of Z-cut single crystal LiTaO3 bulk materials with thicknesses of 27 µm and 250 µm are analyzed. XRD results show characteristic diffraction peaks of Z-cut LiTaO3 at (012), (006), and (202), along with a Ta2O5 peak due to Li-deficiency. The strong (006) peak confirms a high c-orientation, indicating pyroelectric potential. Raman spectroscopy confirms agreement with known vibration modes of bulk $LiTaO_3$. Band gap values for the 27 µm and 250 µm samples are determined as 4.44 eV and 4.65 eV, respectively, with both showing a direct band gap. Temperature changes from 30 °C to 180 °C were applied at rates of 50 °C, 100 °C, and 150 °C. As temperatures rose, negative pyroelectric currents were observed; with cooling, currents shifted positive. The 250 µm thick, 24 mm² $LiTaO_3$ wafer produced about 4 nA at 50 °C rate, rising to 12-13 nA at 150 °C. With larger surface areas yielding higher currents, measurements on three wafers at a 50 °C change showed the highest-area sample producing ~7.5 nA, while the smallest yielded ~0.5 nA. The mean pyroelectric current density was higher in 27 µm (180 µA/m²) than in 250 µm (125 µA/m²), and the pyroelectric coefficient increased with decreasing thickness, measured at 33.43 µC/m²·K (27 µm) and 23.22 µC/m²·K (250 µm). These results suggest the potential of $LiTaO_3$ crystals in IR detectors and self-powered deep UV detector applications due to their wide band gap.

1. INTRODUCTION

Due to rapid advancements in infrared (IR) sensing technology, pyroelectric materials and detectors have garnered significant attention in recent years by virtue of their simple and cost-effective production processes and unique characteristics [1, 2]. Pyroelectric detectors have been extensively studied for a wide range of potential applications, including environmental sensing, security communication, fire prediction, and military services. However, they are frequently used in practical applications such as wavelength selectivity, gas detection, motion sensing, and fire detection [3, 4]. Pyroelectric detectors are constructed from materials in which the orientation of their dipoles' changes with temperature. Pyroelectric materials also exhibit ferroelectric and piezoelectric properties. When such substances are placed between metal electrodes, they form a temperature-sensitive capacitor. If a temperature change occurs, the polarization of the ferroelectric material changes, leading to a time-varying surface charge, and thus the generation of current. In the absence of temperature variation, no current is generated.

* Corresponding author, e-mail: mustafa.buyukharman@ogr.iu.edu.tr

Important pyroelectric materials commonly cited are Lithium Tantalate ($LiTaO_3$), Lead Zirconate Titanate (PZT), Barium Titanate (BTO), and Triglycine Sulfate (TGS). Among these materials, $LiTaO_3$, as can also be seen in Table 1, exhibits a high Curie temperature and a low dielectric constant. It also has a high melting point (1650°C) and is insoluble in water [5]. Studies on thin films $LiTaO_3$ is scarce, as it is typically used in single crystal form and grown by Czochralski method in bulk. Its excellent piezoelectric, pyroelectric, and ferroelectric properties, including a large spontaneous polarization, moderate dielectric constant, low dielectric loss, and a high pyroelectric coefficient, make it a suitable material for pyroelectric IR detectors [1, 6–8]. Recently, potential of pyroelectric materials in self-powered photon detector applications has been also demonstrated [9, 10]. Therefore, being a wide bandgap material, $LiTaO_3$ can be also a candidate for self-powered detectors to be used in the UV region.

Table 1. *Theoretical properties of typical bulk pyroelectric materials*

	Curie temperature (°C)	**Pyroelectric coefficient ($\mu C/m^2K$)**	**Dielectric constant (ε_0)**	**Reference**
$LiTaO_3$	620	180	47	[11–13]
$BaTiO_3$	120	800	2350	[14]
$PbZr_{0.52}Ti_{0.48}O_3$	350	400	500	[15]
TGS	49	250	3323	[16]

Pyroelectric materials are non-centrosymmetric materials, falling within the category of piezoelectric materials. Materials with centrosymmetric possess a single polar axis, which is an axis parallel to the spontaneous polarization of the crystal without any external influence; this spontaneous polarization is found in non-centrosymmetric crystals. In pyroelectric materials, the change in net dipole moment of the material with temperature determines its pyroelectricity. The pyroelectric effect involves the movement of positive and negative charges towards opposite ends of the material when exposed to an electromagnetic wave, as illustrated in Figure 1. Continual exposure to the electromagnetic wave leads to the build-up of static electricity. This property can be harnessed to generate electrical current from various devices [17, 18].

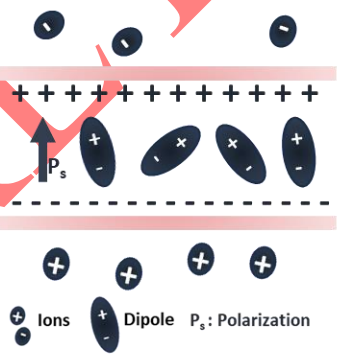

Figure 1. *Schematic representation of spontaneous polarization*

Pyroelectric sensing requires specific material characteristics. The surface of the material should be smooth, and its dielectric loss factor should be low. The dielectric constant is frequency-dependent, which can lead to noise issues; therefore, it should also be low. In pyroelectric materials, as well as in all dielectric materials, it is essential for the material to remain below its Curie temperature to maintain its properties. As the material approaches the Curie temperature, its pyroelectricity decreases and becomes zero at the Curie point. Beyond this temperature, the material loses its characteristics [18].

Figure 2 illustrates the principle behind the generation of current in pyroelectric materials. As shown, pyroelectric current varies with temperature changes. When the temperature increases, the pyroelectric current also increases, and in the case of constant temperature, the pyroelectric current decreases until it reaches zero. This is because maintaining a constant temperature will result in no change, and pyroelectric detectors operate based on temperature fluctuations. Similarly, as the temperature decreases, the direction

of the pyroelectric current changes, increasing in the negative direction. Therefore, changes in pyroelectric current occur with each temperature variation and change in direction [17].

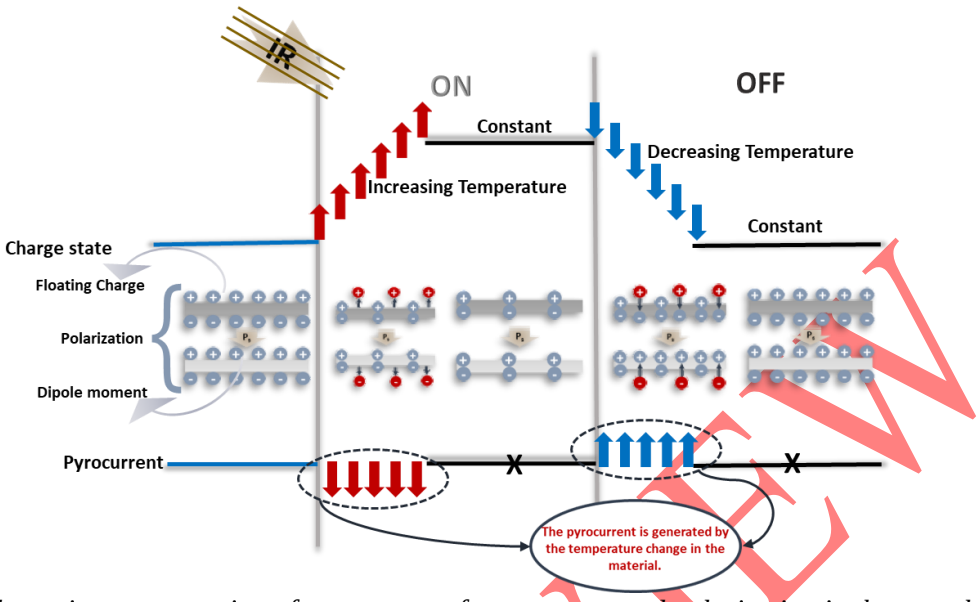

Figure 2. *Schematic representation of occurrence of pyrocurrent and polarization in the pyroelectric material*

The dependence of the pyroelectric coefficient and spontaneous polarization on temperature change is given in Equation (1)

$$\Delta \mathbf{P_s} = \pi dT. \tag{1}$$

The pyroelectric coefficient of the material (p) is a π vector that is equal to the rate of change of spontaneous polarization (P_s) with temperature change (dT) As shown in Figure 2. *Schematic representation of occurrence of pyrocurrent and polarization in the pyroelectric material* and Equation (1), the pyroelectric effect manifests itself as the flow of current in an external circuit connected to the material when the temperature of the material changes. Imagine a thin piece of pyroelectric material with bottom and top electrodes, such that the material has a π component perpendicular to the electrode surfaces and associated with an area A_s. While not all, but many detectors are known to be constructed in a way that the direction of π is perpendicular to the electrode plane, that is, $p = |\pi|$. Therefore, it will be assumed in the subsequent sections that the situation is as such, and the term "pyroelectric coefficient" will be attributed to "p" [17]. The electric current occurs due to the alteration in charge over time, where electric charges flow within a closed circuit, and is defined as [19, 20]

$$i_p = pA_s \frac{dT}{dt}. \tag{2}$$

Here, p is the pyroelectric coefficient, A_s is the electrode overlapping area of the pyroelectric material, and $\frac{dT}{dt}$ is the temperature gradient. It has been reported that pyroelectric properties of pyroelectric materials tend to increase with decreasing sample thickness, therefore a great effort is spent to make the bulk material thinner [21, 22]. So far, most of the studies of bulk $LiTaO_3$ is focused on its pyroelectric properties [11–13, 17, 18], without considering its optical properties.

In this study, structural, optical and pyroelectrical characterization of Z-cut $LiTaO_3$ bulk samples grown by Czochralski method and mechanically thinned to 27 µm and 250 µm are presented. $LiTaO_3$ wafers with thicknesses of 27 µm and 250 µm were cut into different sizes and coated with Pt/Ti bottom and Au/Ti top electrodes to investigate the influence of sample size on pyroelectric properties of $LiTaO_3$.

2. MATERIAL METHOD

There are different methods for pyroelectric current measurements of $LiTaO_3$ single crystal wafers in the literature. The most common of these methods is to perform temperature-dependent current measurements by placing the pyroelectric material-based chip on a plate and heating or cooling it [7]. On the other hand, pyroelectric materials can be heated and cooled in a temperature-controlled chamber and the currents they create at different temperature change rates can be examined. With this technique [19], materials are heated or cooled to the desired temperature with a constant rate of change, while pyroelectric current is measured in response to a constant temperature change over time by operating with a sawtooth signal. In this study, measurements were made by heating and cooling $LiTaO_3$ samples between 30 ℃ and 180 ℃ with a temperature change rate of 50 ℃, 100 ℃ and 150 ℃ using Radiant Technologies Precision LC II ferroelectric parameter analyzer equipped with Linkam T96-S cryostat. It is shown that as the thickness of $LiTaO_3$ decreases, pyroelectric properties improve [23], therefore two samples with thicknesses of 27 µm and 250 µm are investigated in this study. Since the pyroelectric current depends on the area of the pyroelectric material in Equation (2), 250 µm thick $LiTaO_3$ wafer is cut to have 24 mm^2 and 4 mm^2 areas and 27 µm thick $LiTaO_3$ wafer is cut to obtain a 50 mm^2 area, The whole surfaces of $LiTaO_3$ samples were coated with Au/Cr as the front electrode and Pt/Ti as the back electrode with NANOVAK NVEB-600 e-beam evaporator. Before investigation of pyroelectric characteristic, of $LiTaO_3$, structural and optical properties of $LiTaO_3$ were examined using Raman scattering, X-Ray-Diffraction (XRD) and transmittance measurements. Raman scattering analyses was performed using a free-space custom set-up. A 532 nm laser was used excitation source, and the signal was collected using a thermoelectric cooled CCD [24]. XRD measurements were carried out using Rigaku Smartlab X-ray diffraction (XRD) spectrometer at an angular 2θ from 20° to 50° in the increment of 0.02°/minute. Finally, the optical properties of $LiTaO_3$ single crystal wafers were investigated using the Ocean Insight DH 2000 mini spectrometer equipped with a Deuterium & Tungsten Halogen light source.

3. RESULTS

3.1. Structural Characterization

In Figure 3, glancing-angle XRD spectra of $LiTaO_3$ samples with thicknesses of 250 µm and 27 µm are shown. The characteristic peaks of bulk stoichiometric Z-cut $LiTaO_3$ are clearly observed in the spectra, which are indexed according to the XRD card number JCPDS #01-020-0631 [25], which reveals that growth of $LiTaO_3$ is (006) plane- preferential, however observation of diffraction peaks from other planes and Ta_2O_5 shows that the crystal quality of the samples is not good enough. The (006) diffraction peak is responsible for the pyroelectricity of $LiTaO_5$ and observation of the strong (006) peak proves that bulk samples are highly c-oriented and can exhibit pyroelectric characteristics. The peak positions remain approximately the same for both samples. The XRD results reveal the characteristic diffraction peaks of $LiTaO_3$ from (012), (006) and (202) crystal planes together with a characteristic diffraction peak of Ta_2O_5 from (012) plane. The observation of Ta_2O_5- related diffraction peak can be attributed to the Li-deficient growth of the crystal. The peak at 42,44° corresponding to the (202) plane of $LiTaO_3$ is only observed for 250 µm thick samples.

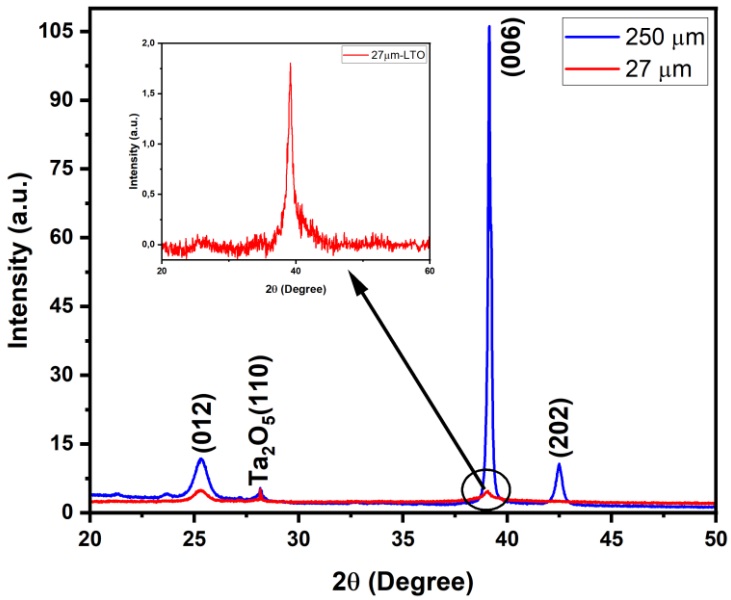

Figure 3. *XRD graphs of 250 µm and 27 µm thick $LiTaO_3$ single crystal wafers*

3.2. Analysis of Raman Scattering

The Raman scattering spectra of single crystal $LiTaO_3$ wafers with thicknesses of 250 µm and 27 µm are presented in Figure 4, covering the range of 230 to 1160 cm^{-1}. The characteristic Raman active modes of $LiTaO_3$ are observed in the spectra [26].The peak positions are approximately the same for each sample. For the 27 µm thickness $LiTaO_3$ sample, the peaks are observed at 256 cm^{-1} (3E TO), 314 cm^{-1} (4E TO), 355 cm^{-1} ($2A_1$ LO), 381 cm^{-1} (5E LO), 405 cm^{-1} (3A1 LO), 462 cm^{-1} (7E TO), 591 cm^{-1} (8E TO), 661 cm^{-1} (9E TO), and 864 cm^{-1} ($4A_1$ LO) [27, 28]. Here, TO represents transverse optic polar oscillations, while LO represents longitudinal optic polar oscillations. The peak at 749 cm^{-1} is attributed to the fundamental doubly degenerate E(TO) and E(LO) symmetry-type vibrations perpendicular to the polar axis of $LiTaO_3$ [29]. The peaks of the 250 µm thick $LiTaO_3$ sample are observed at the same wavenumber values with higher peak intensities, as expected. However, the LO peak at 381 cm^{-1} is not observed.

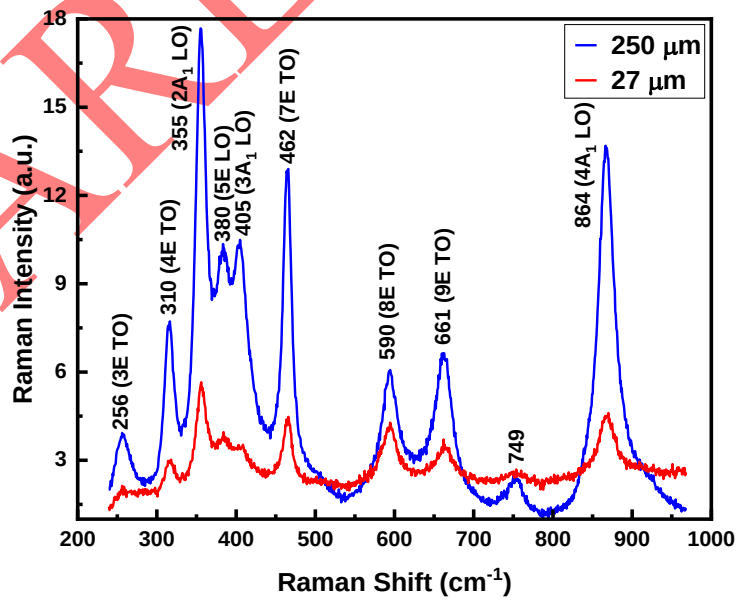

Figure 4. *Raman graphs of 250 µm and 27 µm thick $LiTaO_3$ single crystal wafers*

3.3. Optical Characterization

Transmittance measurements were conducted in the wavelength range of 250-1100 nm. As can be seen from Figure 4, the transmittance (≥300 nm) of 27 µm thick $LiTaO_3$ is over 70% and is 3 times higher than the 250 µm thick sample. The bandgap value was determined from Tauc's equation. If the intensity of the incoming photons onto a film of thickness *t* is I_0 and the wavelength of incoming photons is λ, the intensity of the transmitted light is defined as,

$$I_t = I_0 e^{-\alpha t}. \quad (3)$$

where α is absorption coefficient and the band gap is calculated using Tauc's equation given as [30],

$$\alpha h\nu = A\left(h\nu - E_g\right)^{\gamma}. \quad (4)$$

Using the obtained transmittance results, the band gap values of $LiTaO_3$ wafer were determined by Tauc plot analysis. The wavelenght dependence of absorption coefficient as well as Tauc's plot is presented in Figure 5. The best fit to the experimental data is obtained for γ =2, which indicates $LiTaO_3$ is a direct band gap material. The band gap values of 250 µm and 27 µm thick $LiTaO_3$ single crystal wafers calculated with the Tauc plot are 4.69 eV and 4.44 eV, respectively. There is no reported bandgap value of bulk $LiTaO_3$, however the obtained band gap values are higher than the reported ones for the $LiTaO_3$ thin films [31].

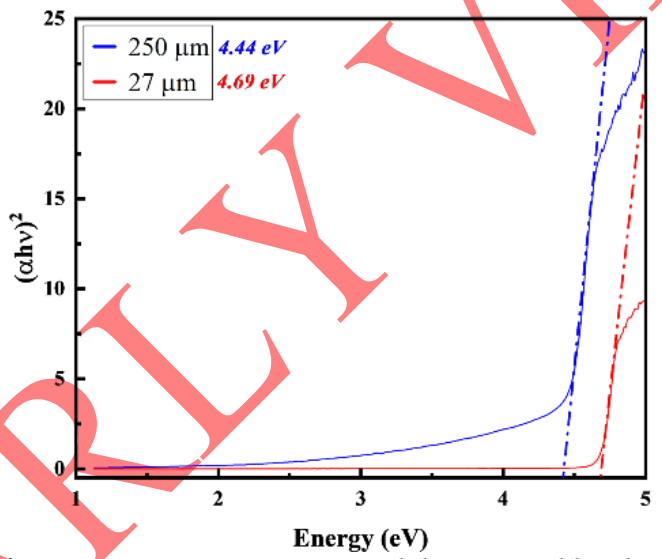

Figure 5. *Tauc's plot of transmittance measurements and the extracted band gap of 250 µm and 27 µm thickness $LiTaO_3$ single crystals*

3.4. Pyroelectric Characterization

In Figure 6, generated pyroelectric current in $LiTaO_3$ samples at different temperature change rates are shown. While a pyroelectric current of approximately 3 nA was generated in a 250 µm thick 24 mm^2 $LiTaO_3$ sample with a temperature change rate of 50 °C, the generated pyroelectric current at a temperature change rate of 150 °C increases to approximately 11 nA. As the temperature change rate increases to three-fold from 50 °C to 150 °C (Figure 6b), the pyroelectric current also increases linearly at the same rate as expected in Equation (2).

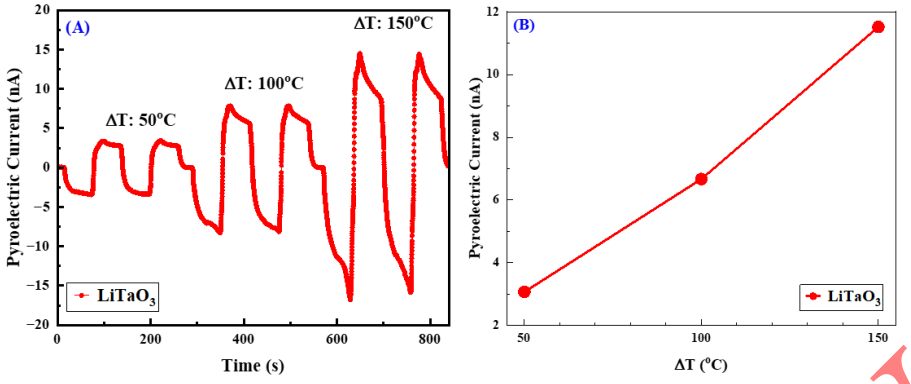

Figure 6. *(a) Pyroelectric current graphs of $LiTaO_3$ samples with 250 µm thickness and 24 mm^2 area at different temperature change rates, (b) mean pyroelectric current at different temperature changes*

Since the generated pyroelectric current depends on the area and the thickness of pyroelectric material, pyroelectric characterization was carried out on three different $LiTaO_3$ samples, 250 µm thick with 24 mm^2 and 4 mm^2 area and 27 µm thick with 50 mm^2 area, at a temperature change rate of 50 °C. Figure 7 shows the pyroelectric current measurement results of $LiTaO_3$ samples of different sizes. The highest pyroelectric current value is observed for 27 µm thick sample.

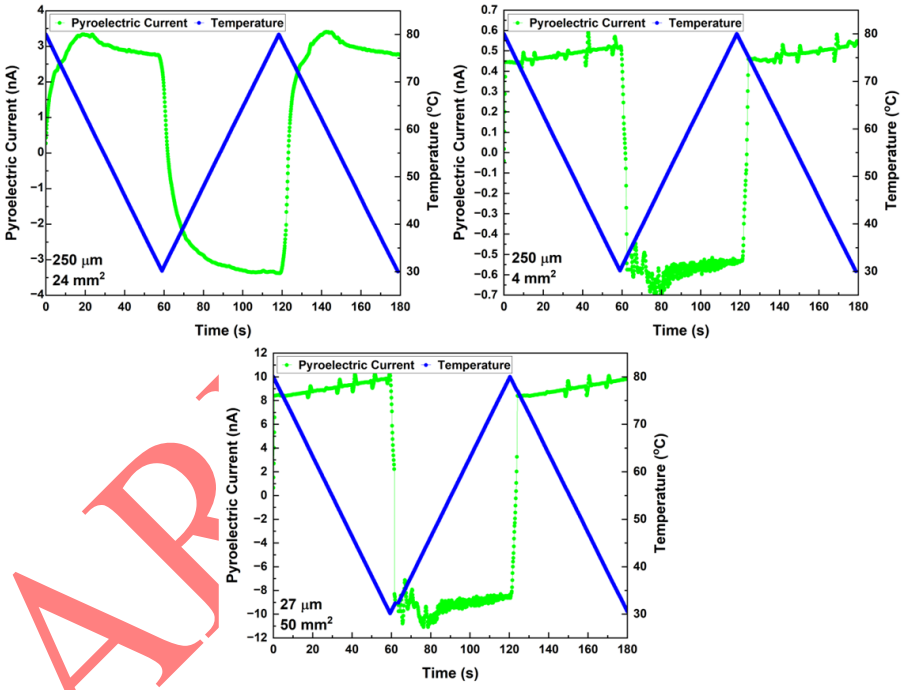

Figure 7. *Pyroelectric current graphs of $LiTaO_3$ samples with different sizes at a 50 °C temperature change rate*

Based on the data presented in Figure 7, Pyroelectric current density was calculated for the samples with a thickness of 250 µm (area 4 mm^2) and 27 µm (area 50 mm^2) as seen in Figure 8a and 8b, respectively. A slightly higher pyroelectric current density is obtained for 27 µm thick sample. Using pyroelectric current density in Equation (2), the mean values of pyroelectric coefficient of the 27 µm and 250 µm thick samples are determined as 33.43 $\mu C/m^2 \cdot K$ and 23.22 $\mu C/m^2 \cdot K$, respectively. During the heating-cooling cycle, pyroelectric current tends to increase not constant therefore the mean value of the pyroelectric current is taken to calculate pyroelectric coefficient. The pyroelectric coefficient tends to be higher for the thinner bulk $LiTaO_3$, which agrees with the literature [32]. The obtained values of pyroelectric coefficient of the samples is found to be about one-sixth lower than the reported theoretical value of bulk $LiTaO_3$ given in Table 1, which can be related to insufficient single crystal quality as discussed in XRD results. Our results reveals that the bulk 27 µm thick $LiTaO_3$ sample is more promising to be used in thermal detector applications.

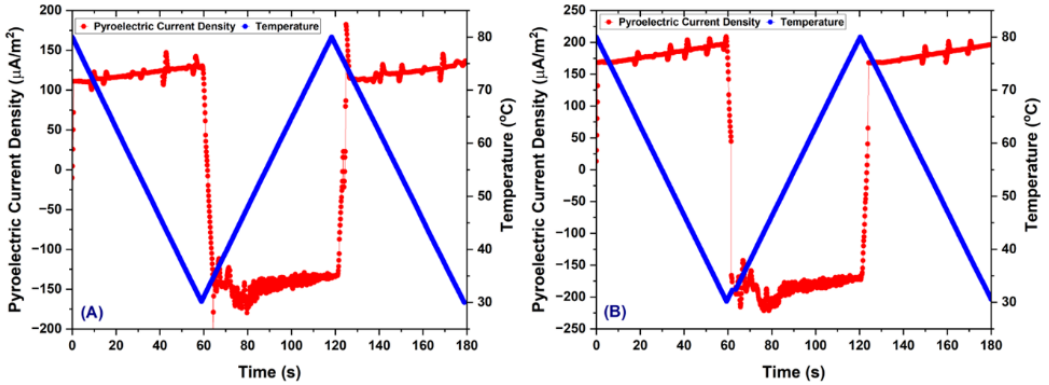

Figure 8. *Pyroelectric current density graphs of (a) 250 μm and (b) 27 μm thick $LiTaO_3$ samples at a 50 °C temperature change rate*

4. CONCLUSION

The structural, optical, and pyroelectrical properties of bulk single crystal Z-cut $LiTaO_3$ samples with different thicknesses (250 μm and 27 μm) have been investigated. XRD results has confirmed that bulk $LiTaO_3$ is c-oriented with a strong (006) peak. The observation of other XRD peaks is an indication of por crsyal quality. Raman scattering results have exhibited the characteristic of bulk $LiTaO_3$ crystal. As for thinner $LiTaO_3$ sample, intensity of both Raman scattering and XRD peaks has been found to be lower. The band gap of the samples obtained as 4.69eV (27 μm) and 4.44 eV (270 μm) indicates $LiTaO_3$ has potential to be used in self-powered deep-UV detectors thanks to its wide band gap. The mean value of pyroelectric current density of approximately 180 $\mu A/m^2$ measured from 27 μm thick $LiTaO_3$ sample can be promising to use the sample as an active material of a pyroelectric detector.

ACKNOWLEDGEMENT

This work is supported by The Scientific and Technological Research Council of Türkiye (TUBITAK) 2244 – Industrial PhD Fellowship Program (Project Number: 118C117).

CONFLICTS OF INTEREST

No conflict of interest was declared by the authors.

REFERENCES

[1] Dinh T. V., Choi I. Y., Son Y. S., and Kim J. C., “A review on non-dispersive infrared gas sensors: Improvement of sensor detection limit and interference correction”, Sensors and Actuators, B: Chemical, 231, 529–538, (2016).

[2] Rogalski A., “Infrared detectors: Status and trends”, Progress in Quantum Electronics, 27, 59–210, (2003).

[3] Jun L., Qiulin T., Wendong Z., Chenyang X., Tao G., and Jijun X., “Miniature low-power IR monitor for methane detection”, Measurement (Lond), 44, 823–831, (2011).

[4] Qiu-lin T., Wen-dong Z., Chen-yang X., Ji-jun X., Jun L., Jun-hong L., and Ting L., “Design, fabrication and characterization of pyroelectric thin film and its application for infrared gas sensors”, Microelectronics Journal, 40(1), 58–62, (2009).

[5] Estrada R., Djohan N., Pasole D., Dahrul M., Kurniawan A., Iskandar J., Hardhienata H., and Irzaman, “The optical band gap of LiTaO3 and Nb2O5-doped LiTaO3 thin films based on Tauc Plot method to be applied on satellite”, IOP Conference Series Earth Environmental Science, 54, 012092, (2017).

[6] Kao M.C., Chen H.Z., Young S.L., Lin C.C., and Yu C.C., "Thickness-dependent microstructures and electrical properties of LiTaO3 thin films prepared by a sol-gel process", International Journal of Modern Physics B., 21(18), 3404-3411, (2007).

[7] Levine B.F., "Quantum-well infrared photodetectors", Journal of Applied Physics, 74, R1, (1998).

[8] Stenger V., Shnider M., Sriram S., Dooley D., and Stout M., "Thin Film Lithium Tantalate (TFLT) pyroelectric detectors", Proceedings of SPIE – The International Society for Optical Engineering, 8261, 174–182, (2012).

[9] Chen M., Shen X., Zhou C., Cao D., and Xue W., "High-performance self-powered visible-blind ultraviolet photodetection achieved by ferroelectric $PbZr_{0.52}Ti_{0.48}O_3$ thin films", Journal of Alloys and Compounds, 897, 163202, (2020).

[10] Ma N., and Yang Y., "Enhanced self-powered UV photoresponse of ferroelectric $BaTiO_3$ materials by pyroelectric effect", Nano Energy, 40, 352-359, (2017).

[11] Kovar M., Dvorak L., and Cerny S., "Application of pyroelectric properties of LiTaO3 single crystal to microcalorimetric measurement of the heat of adsorption", Applied Surface Science, 74(1), 51-59, (1994).

[12] Muralt P., "Micromachined infrared detectors based on pyroelectric thin films", Reports on Progress in Physics, 64, 1339, (2001).

[13] Xiao X., Liang S., Si J., Xu Q., Zhang H., Ma L., Yang C., and Zhang X., "Performance of LiTaO3 Crystals and Thin Films and Their Application", Crystals, 13(8), 1233, (2023).

[14] Deb K.K., Hill M.D., and Kelly J.F., "Pyroelectric characteristics of modified barium titanate ceramics", Journal of Materials Research and Technology, 7, 3296–3305, (1992).

[15] Zhao H., Liu X., Ren W., and Zhang Y., "Preparation and characterization of lead zirconate titanate thin films grown by RF magnetron sputtering for pyroelectric infrared detector arrays", Ceramic International, 44, 7-10, (2018).

[16] Sinha N., Goel N., Singh B.K., Gupta M.K., and Kumar B., "Enhancement in ferroelectric, pyroelectric and photoluminescence properties in dye doped TGS crystals", Journal of Solid State Chemistry, 190, 180–185, (2012).

[17] Muralt P., "Pyroelectricity", Encyclopedia of Condensed Matter Physics, 441–448, (2005).

[18] Lang S.B., "Pyroelectricity: From Ancient Curiosity to Modern Imaging Tool", Physics Today, 58, 31, (2007).

[19] Lubomirsky I., and Stafsudd O., "Invited review article: Practical guide for pyroelectric measurements", Review of Scientific Instruments, 83, 5, (2012).

[20] Ranu, U.B., Sinha R., and Agarwal P.B., "CMOS compatible pyroelectric materials for infrared detectors", Materiat Science and Semiconductor Processing, 140, 106375, (2022).

[21] Hang W., Zhou L., Zhang K., Shimizu J., and Yuan J., "Study on grinding of LiTaO3 wafer using effective cooling and electrolyte solution", Precision Engineering, 44, 62-69, (2016).

[22] Schossig M., Norkus V., and Gerlach G., "Dielectric and pyroelectric properties of ultrathin, monocrystalline lithium tantalate", Infrared Physics and Technology, 63, 35-41, (2014). DOI: https://doi.org/10.1016/j.infrared.2013.12.005

[23] Yan, T., Zheng, F., Yu, Y., Qin, S., Liu, H., Wang, J., and Yu, D., "Formation mechanism of black LiTaO3 single crystals through chemical reduction", Journal of Applied Crystallography, 44, 158–162, (2011).

[24] Durdu, S., Aktas, S., Sarcan F., Akagunduz, E., Gultekin, B. Erol, A., Usta, M., "Effect of water-based electrolyte on surface, mechanical and tribological properties of ZrO_2 nanotube arrays produced on zirconium", Journal of the Australian Ceramic Society, 60, 833–848, (2024).

[25] Vilarinho P.M., Barroca N., Zlotnik S., Félix P., and Fernandes M.H., "Are lithium niobate (LiNbO3) and lithium tantalate (LiTaO3) ferroelectrics bioactive?", Materials Science and Engineering: C, 39, 395–402, (2014).

[26] Kostritskii S.M., Aillerie M., Bourson P., and Kip D., "Raman spectroscopy study of compositional inhomogeneity in lithium tantalate crystals", Applied Physics B, 95, 125–130, (2009).

[27] Abdurakhmonov S.D., and Gorelik V.S., "Overtone Raman Scattering in Lithium Tantalate Single Crystals", Optical Spectroscopy, 127, 587–590, (2019).

[28] Sanna S., Neufeld S., Rüsing M., Berth G., Zrenner A., and Schmidt W. G., "Raman scattering efficiency in LiTaO3 and LiNbO3 crystals", Physical Review B Condensed Matter and Material Physics, 91, 224302, (2015).

[29] Palatnikov M., Sidorov N., Pyatyshev A., and Skrabatun A., "Comparison of Raman Spectra of Optically Nonlinear LiTaO3:Cr3+ (0.005 wt%) Crystal Laser Excited in Visible (532 nm) and Near-IR (785 nm) Areas", Photonics, 10, 439, (2023).

[30] Tauc J., Grigorovici R., and Vancu A., "Optical Properties and Electronic Structure of Amorphous Germanium", Physica Status Solid (b), 15, 627–637, (1966).

[31] Ismangil A., Jenie R.P., Irmansyah, and Irzaman, "Development of Lithium Tantallite (LiTaO3) for Automatic Switch on LAPAN-IPB Satellite Infra-red Sensor", Procedia Environmental Sciences, 24, 329–334, (2015).

[32] Stokowski S., Venables J., Byer N., and Ensign T., "Ion-beam milled, high-detectivity pyroelectric detectors", Infrared Physics, 16 (3): 331–334, (1976).